Self-Referenced Smartphone-Based Nanoplasmonic Imaging Platform for Colorimetric Biochemical Sensing

Xinhao Wang,[†,‖] Te-Wei Chang,[†,‖] Guohong Lin,[†] Manas Ranjan Gartia,*[,‡] and Gang Logan Liu*[,†,§]

[†]Micro and Nanotechnology Laboratory, Department of Electrical Engineering, University of Illinois at Urbana−Champaign, Urbana, Illinois 61801, United States

[‡]Department of Mechanical and Industrial Engineering, Louisiana State University, Baton Rouge, Louisiana 70803, United States

[§]School of Life Science and Technology, Huazhong University of Science and Technology, Wuhan, Hubei 430074, China

S *Supporting Information*

ABSTRACT: Colorimetric sensors usually suffer due to errors from variation in light source intensity, the type of light source, the Bayer filter algorithm, and the sensitivity of the camera to incoming light. Here, we demonstrate a self-referenced portable smartphone-based plasmonic sensing platform integrated with an internal reference sample along with an image processing method to perform colorimetric sensing. Two sensing principles based on unique nanoplasmonics enabled phenomena from a nanostructured plasmonic sensor, named as nanoLCA (nano Lycurgus cup array), were demonstrated here for colorimetric biochemical sensing: liquid refractive index sensing and optical absorbance enhancement sensing. Refractive indices of colorless liquids were measured by simple smartphone imaging and color analysis. Optical absorbance enhancement in the colorimetric biochemical assay was achieved by matching the plasmon resonance wavelength with the chromophore's absorbance peak wavelength. Such a sensing mechanism improved the limit of detection (LoD) by 100 times in a microplate reader format. Compared with a traditional colorimetric assay such as urine testing strips, a smartphone plasmon enhanced colorimetric sensing system provided 30 times improvement in the LoD. The platform was applied for simulated urine testing to precisely identify the samples with higher protein concentration, which showed potential point-of-care and early detection of kidney disease with the smartphone plasmonic resonance sensing system.
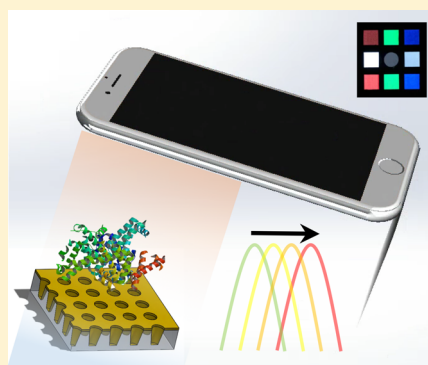
Noble metallic nanostructures have been demonstrated to be used in the application of biological sensing,[1,2] imaging,[3,4] and energy harvesting[5,6] in recent years, mainly due to the advantage of their unique plasmonic property. Noble metals show collective electromagnetic resonance due to their negative refractive index in the visible range, which leads to surface plasmon resonance (SPR) or localized surface plasmon resonance (LSPR).[7,8] Both SPR and LSPR techniques are widely used for label-free biological sensing.[9−12] Compared with the classical Krestchmann configuration, which involves complex prism integration,[13] a noble metallic nanostructure is more adaptive to be integrated in portable devices to achieve point-of-care applications.[14] Another advantage of plasmonic nanostructure is the ability to perform colorimetric sensing, generally due to its relatively large wavelength shift as refractive index changes. Although quite a few sensing devices have been demonstrated for refractive index sensing (resonance peak wavelength shift sensing), they suffer from either relative low sensitivity[12,15] or resonance wavelength beyond the visible region.[16] Compared with chemical binding-based colorimetric sensing,[17,18] plasmonic colorimetric sensing provides advantages such as faster readout,[14] elimination of chemical preparation, or mitigating other limitations such as vapor pressure and chemical flow control, which brings additional

complexities, for example, in colorimetric gas sensing.[19] In terms of point-of-care applications, several groups have developed portable platforms using commercial sensors and image processing methods to do colorimetric sensing, but the sensor lacks a lower limit of detection (LoD), as required for sensitive biofluids detection.[20−22] Further, in order to achieve repeatability and reliability in the measurements, the sensors require a reference sample (sensor with standard colorimetric properties) to account for the variation in light source intensity, type of light source, Bayer filter algorithm, and sensitivity of the camera to incoming light.

In this paper, we demonstrated a self-referenced portable nanoplasmonic imaging platform for colorimetric biomolecule sensing, by using an image processing method under well-controlled optical imaging conditions. Unlike a classical extraordinary optical transmission (EOT) structure, which usually gives rise to multiple spectrum features,[23] the transmission spectrum of our plasmonic device has its single resonance wavelength in the visible light region.[24] We are able to demonstrate colorimetric sensing with a refractive index

change due to its SPR and LSPR phenomena.[24,25] The mechanism of improved limit of detection for biomolecules quantification is due to the matching of the resonance wavelength of the sensor after refractive index change to that of the absorbance wavelength of the analyte. Absorbance is, thus, enhanced at this resonance wavelength under amplified electromagnetic intensity near the substrate surface.[26] The portable plasmonic platform showed about a two-order of magnitude improvement in sensitivity on a microplate reader and a much lower LoD compared to other portable platforms using commercial chemical testing strips.

MATERIALS

Plasmonic nanohole sensor. Norland Optical Adhesive 61 (NOA 61) was used as UV curable polymer in this paper. NOA 61 is a transparent liquid photopolymer, which can be cured by ultraviolet light with maximum absorption within the range 320−380 nm with peak sensitivity around 365 nm. Optically transparent and flexible polyethylene terephthalate (PET) film with the thickness of 250 μm was used as the substrate for the UV curing nanoreplica process. The UV curing process was done with a Dymax 2000-EC UV curing flood lamp, which was designed to effectively limit output energy to longwave (UVA) for general purpose, low-intensity curing of UV adhesives, coatings, and inks.

Before the nanoreplica process, a glass master mode with nanocone arrays was first immersed into dimethyldichlorosilane ($Si(CH_3)_2Cl_2$) solution for 30 min. The periodicity, height, and width of nanocone are 350, 500, and 200 nm separately. The mold was then rinsed with DI water and ethanol to form a monolayer of saline on the surface. The hydrophobic saline surface helps the removal of UV-curable polymer (NOA-61) and ensures the validity of pattern transfer. After evenly spreading ~10 μL of UV-curable polymer on the nanocone surface, constant UV light with power density of 105 mW cm^{-2} was applied to the substrate for solidification. An E-beam evaporation system was used after replication for metal deposition on the polymer nanostructure. The deposition was performed in a sequence of Ti (9 nm) and Au (90 nm) with rate controlled at 1 Å s^{-1} to ensure uniformity. The nanostructure of nanoLCA could be found in Figure 1a.

Glycerol. Glycerol (Sigma-Aldrich, for molecular biology, >99%) was used for measuring the resonance peak shift with the change of surrounding material due to its stable refractive index change with the solution concentration.

Coomassie (Bradford) protein assay reagent kit. In order to measure the concentration level of BSA, the Coomassie protein assay reagent kit (Thermo Scientific) was used. The Coomassie Protein Assay Kit is a quick and ready-to-use colorimetric method for total protein quantitation which was modified from the well-known Bradford Coomassie-binding assay. When Coomassie dye binds protein in an acidic medium, an immediate shift in absorption maximum occurs from 465 to 595 nm with a concomitant color change from brown to blue. It can be performed in either test tube or microplate format. Protein concentrations are estimated by reference to absorbance obtained for a series of standard protein dilutions, which are assayed alongside the unknown samples.

BSA. Bovine Serum Albumin (BSA, Sigma-Aldrich, lyophilized powder, >96%) was dissolve in the DI water to simulate different levels of concentration for total protein testing.

Artificial urine sample (A, B, C, D). A urinalysis simulated urine kit was used to anaylze the practicality of the sensing system for biological testing. The kit contains four different testing samples, which are labeled as control, patient A, patient B, and patient C. Control (D) was used as the reference to compare with three other samples, which had certain specific molecules exceeding the normal human body concentration. Patients A, B, and C indicated to glucose, protein, and calcium under abnormally high concentration levels, respectively.

Microplate reader. A Biotek Synergy HT microplate reader was used to prove the capability of the plasmonic nanohole sensor on self-referenced sensing. The Synergy HT Multidetection reader is a robotic-compatible microplate reader that can measure absorbance, fluorescence, and luminescence.

Smartphone. The testing smartphone used in this paper was an Apple iPhone 6, which contains an 8-megapixel camera with a largest aperture as f/2.2. In order to have consistent exposure conditions within all the images, the application software called Manual was used. It can manually tune the exposure parameters such as shuttering time and aperture.

EXPERIMENTAL METHODS

Bradford assay preparation. A standard microplate protocol was used for the preparation of the experiment. For the protein concentration within the range of 100−1500 μg/mL, 5 μL of each sample was added into the appropriate microplate wells. 250 μL of the Coomassie Reagent was then added to each well and mixed with a plate shaker for 30 s. If the protein concentration was low (in the range of 1−25 μg/mL), 150 μL of each sample was added to microplate wells, followed by 150 μL of the Coomassie Reagent. After shaking for 30 s, all of the samples were incubated for 10 min at room temperature for the most consistent results.

Absorbance measurement with microplate reader. Absorbance spectrum (400−800 nm) was measured for Bradford assay with and without nanoLCA substrate for comparison. The standard protein solution set prepared as reference has a concentration range of 0.001−4 mg/mL. Absorbance at 595 nm was also measured for prepared assay with and without nanoLCA.

Smartphone platform setup. A portable platform was made for smartphone colorimetric sensing. A flat-surface white LED background was used to illuminate the sample area, assisting the camera at the top of the platform to capture the
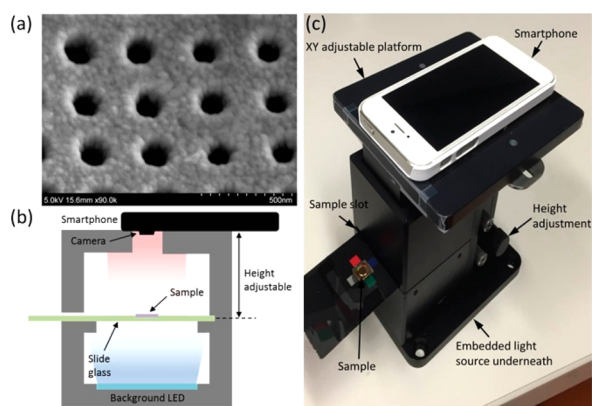

Figure 1. Smartphone based portable colorimetric sensing platform. (a) SEM image of nanoLCA. (b) Schematic of internal optical detection system setup. (c) Real image of optical detection setup.

uniform transmission image. (Figure 1b) The testing sample was injected inside a PDMS (polydimethylsiloxane) micro-cavity embedded with a nanoLCA substrate at the bottom. The whole plasmonic device was supported by a piece of glass slide, which enabled easy removal/insertion to the portable platform. Standard square color patterns (red (255,0,0), green (0,255,0), and blue (0,0,255)) were printed around the PDMS micro-cavity for color calibration. In order to block light underneath transmitting the whole glass slide, a plastic sheet with printed as black except the sensing and calibration regions was used to eliminate the interference of transmission light from the region besides the sensing area. The glass slide with sample was inserted through the sample slot at the side of the portable platform. The top of the platform could be adjusted horizontally in the $X-Y$ plane while the height of the smartphone could also be adjusted to fit the focal length (Figure 1c).

An iOS application was used for capturing the transmission image from a smartphone device. The application enabled the controllability of the values of camera settings such as ISO, exposure time, white balance, and gain factor, which helped to provide a consistent exposure condition in image analysis. The parameters for portable platform sensing were set as ISO = 100; S (exposure time) = 1/30 s; gain = 1.5; white balance = 5100 K.

Image analysis method. The intensities of the red (R), green (G), and blue (B) channels were retrieved separately from the transmission image. The RGB values from a tested sample were calibrated according to the standard RGB transmission images next to the sample. These standard RGB transmission images were only used to calibrate their corresponding channel.

■ RESULTS AND DISCUSSION

Portable colorimetric sensing using refractive index change. Due to plasmon−molecule interaction and the increase in polarizability of the plasmons, a red shift in the resonance peak is expected with the increase of the refractive index of the surrounding medium.[24,25] (Figure 2a) The resonance peaks in the transmission spectrum of the plasmonic sensor are mainly due to the surface plasmon polariton-Bloch wave (SPP-BW) mode[27−29] and localized surface plasmon resonance (LSPR) from the Mie scattering model,[30] which has been discussed in our previous work.[24,25] To characterize the performance (sensitivity) of the nanoLCA device on the portable platform, glycerol solutions with different concentrations (0%, 10%, 20%, 30%, 40%) were used to map the surrounding refractive index range from 1.333 to 1.384 (the expected range of typical biological fluids at low concentration). The images taken from the smartphone showed a color change to more bluish with the increase in glycerol concentration (Figure 2b). The RGB color space method was used here instead of HSV since HSV was applicable for devices with a single peak wavelength shift under a uniform light source; in contrast, neither the device's transmission spectrum nor the LED light source spectrum was so ideal in our case. The RGB channels were normalized according to the standard RGB color patterns captured on the same image. The equation for normalization (red channel for example) could be expressed as $R_{norm} = \dfrac{R_{sample}}{R_{red\ pattern}} \times 255$. This normalization step overcomes the imperfectness of the reference color patterns due to plastic reflection and ink absorption. Since RGB values could be considered as a vector in three-dimensional color space, the
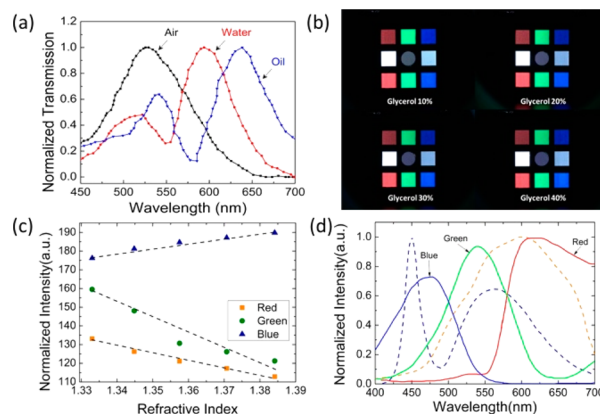

Figure 2. Sensing using refractive index change. (a) Normalized transmission spectrum of air, water, and oil from nanoLCA. (b) Images taken from glycerol at different concentrations (10%, 20%, 30%, 40%) on a nanoLCA substrate from the current optical platform. (c) Normalized intensity change of RGB channels with refractive index change when white LED was used as background light source. (d) Normalized spectrum of white LED and light source from Princeton Instrument. (The dashed blue curve was the spectrum of white LED, while the dashed orange curve was the spectrum of the light source from Princeton Instrument.) RGB spectral sensitivity from a typical image sensor (solid curve).

light source intensity is proportional to the norm of such a vector. So, one more normalization step was performed as $R'_{norm} = \dfrac{R_{norm}}{\sqrt{R_{norm}^2 + G_{norm}^2 + B_{norm}^2}} \times \sqrt{3 \times 255^2}$, in order to cancel out the variation of light source intensity in every image captured. This method acted as an internal reference and circumvented any effect of variation in light source intensity, type of light source, Bayer filter algorithm, and sensitivity of the camera to incoming light on the acquired images. This portable platform showed good linear correlation with different concentrations of glycerol in RGB channels (Figure 2c). The normalized color intensity in RGB channels was mainly affected by the light source spectrum, the transmission spectrum of nanoLCA substrate, and the spectral sensitivity of the RGB channels in the camera. A typical spectral sensitivity from the commercial image sensor (Sony) is shown in Figure 2d, where the spectra of RGB channels are mainly defined by pixel filters in the image sensor. In Figure 2c, although the blue channel displayed the highest intensity owing to the sharp dominant peak at 450 nm from the white LED light source (Figure 2d), the smallest amount of change was found because of the relative small change at the blue region in nanoLCA's transmission spectrum. The red channel should be most sensitive from the aspect of the transmission spectrum, but the green channel actually showed the highest sensitivity. The combination of red shift of the transmission spectrum and red channel sensitivity should lead to an increase in red channel intensity, but it contradicted with the decrease in the red region from the light source. The green channel, instead, showed a decreasing trend in both spectral sensitivity and light source with the red shift in the transmission spectrum, which made it the most sensitive channel for characterization. From the above discussion, it is obvious to see that the light source spectrum and image sensor's spectral sensitivity play an important role when analyzing colorimetric images changing with resonance peak shift.

Portable colorimetric sensing using absorbance enhancement. The sensing mechanism with nanoLCA is not limited to refractive index change. The local enhanced electromagnetic field near the nanostructure surface would assist sensing at the lower limit of detection. First, absorbance enhancement of nanoLCA was verified with a Bradford assay and BSAs on a microplate reader. Since the bound dye to protein in the Bradford assay has an absorption spectrum maximum at 595 nm, wavelength was fixed at 595 nm in the microplate reader to compare the absorbance with and without nanoLCA. The absorbance without nanoLCA shows (Figure 3a
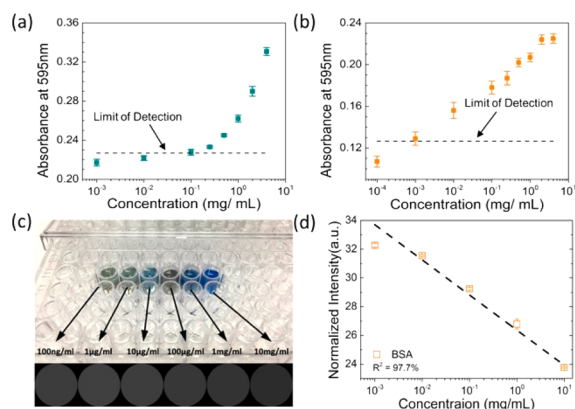

Figure 3. Sensing using absorbance enhancement. (a) Limit of detection without nanoLCA in terms of absorbance at 595 nm. (b) Limit of detection with nanoLCA in terms of absorbance at 595 nm. (c) Bradford assay test of BSA at various concentrations (100 ng/mL ~ 10 mg/mL) and corresponding intensity of the red channel in the gray scale. (d) Normalized intensity of the red channel with the change of BSA concentration.

and Figure 3b) its LoD (Limit of Detection) for BSA quantization at 0.1 mg/mL while the LoD with nanoLCA can achieve 0.001 mg/mL, which is 100 times more sensitive (Supporting Information (SI)).[31] It was already illustrated that the transmission spectrum of nanoLCA with solution media (water) showed a dominant peak at around 600 nm (Figure 2a). The absorbance enhancement is mainly due to this plasmonic resonance wavelength of nanoLCA in the transmission spectrum matching with the absorbance peak wavelength of the bound dye in the Bradford assay (595 nm in this case).[26] The enhanced localized electrical field at the resonance wavelength facilitates the additional light absorption of the bound dye.

Since the absorbance spectrum has its peak wavelength in the red region, white LED with low red intensity is not a suitable light source. Another light source (halogen light) from Princeton Instrument with the peak around 600 nm was used to achieve higher image intensity (Figure 2d). The red channel should be the most sensitive channel and will be proportional to the protein concentration. So the change of intensity of the red channel was applied to the image analysis on the portable colorimetric sensing platform. Bradford assay with BSA was added separately to the microfluid chamber on the portable platform, from 100 ng/mL to 10 mg/mL. The volume of the microfluid chamber is only 20 μL, which is much smaller than the volume in the 96 well plate (255 or 300 μL). The intensity of the channel was retrieved from the image taken by a smartphone and normalized (calibrated) using the standard color patterns around the sample area. The intensity of the red

channel was normalized only with the standard red color pattern, since the standard green and blue patterns show much less intensity, which is not stable and may cause larger error due to the noise. The normalized intensity of the red channel was scaled two times larger to enhance comparison and displayed in the gray image (Figure 3c, bottom). It showed a linear correlation with the concentration in the logarithmic scale (Figure 3d). The coefficient of determination (R^2) was 0.97. The intensity of the red channel decreased with the increase of BSA concentration because of the higher absorbance in the red color region. Since intensity saturation was observed at 0.001 mg/mL, the LoD obtained with the image processing method was close to 0.01 mg/mL, which was larger than that obtained from the microplate reader. This is probably due to either higher sensitivity of the optical sensor in the bulk instrument or the shorter optical path compared with the 96 well plate. Shorter optical path leads to much smaller change in transmission according to the Beer–Lambert law, which illustrates an exponential relation between transmission and optical depth. In comparison with the case without nanoLCA, it was demonstrated that higher sensitivity and better linearity can be achieved with nanoLCA (Supporting Information (SI) Figure S1) Compared with commercial protein testing strips, which normally showed LoD at 0.3 mg/mL (Supporting Information (SI) Figure S2), an enhancement of about 30 times in LoD was achieved on our portable sensing platform.

Application for urine testing. Protein concentration measurement in urine is often used as a criterion to identify proteinuria, a disease caused by kidney failure.[32] Four samples from artificial urine were used to simulate the identification of such kidney disease by a self-referenced portable sensing platform. These four samples indicate abnormal glucose, protein, calcium, and reference, respectively. All of them were combined with a Bradford assay using a high concentration protocol and tested with the same procedure as described above. Due to the device's resonance mode matching with the bound dye's absorbance peak at 595 nm, the selectivity for detecting the specific protein in a urine sample was achieved. The intensity of the red channel from sample image was normalized according to the standard red color pattern and scaled four times larger in the gray scale to enhance comparison (Figure 4a). The retrieved color intensity from sample B looks
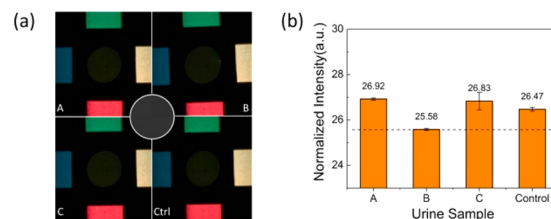

Figure 4. Urine sample testing. (a) Color images taken for urine sample testing, and corresponding intensity (×4) of the red channel in the gray scale. (b) Bar chart of normalized intensity in the red channel for different urine samples.

darker than that from other samples. The normalized intensity from sample B is much smaller than other samples, indicating that sample B has a higher concentration of protein (Figure 4b). Therefore, this portable colorimetric platform provided a solution for quick diagnosis of kidney failure related diseases.

CONCLUSIONS

In summary, a self-referenced portable colorimetric sensing platform has been demonstrated. The system works on the principles of refractive index change and absorbance enhancement. In refractive index sensing application, characterization of the sensor substrate was made using an image processing method by self-referenced normalization. The effect of light source and spectral sensitivity on intensity change was analyzed. It was shown that the most sensitive channel satisfied the same tendency in both light source and spectral sensitivity with a resonance peak shift in the transmission spectrum. In the case of absorbance enhancement application, Bradford assay was used to quantify protein concentration due to the match of the absorbance peak wavelength of the dye with the plasmonic resonant wavelength, where an electric field with a higher intensity near the substrate surface facilitated light absorption. Sensitivity was thus improved by 100 times in the microplate reader format. Improvement of about 30 times in LoD was also achieved compared to other commercial protein testing strips. A urine test was then performed to show the ability of our platform to diagnose kidney failure by identifying protein concentration at abnormal levels with specificity. Our platform also showed potential and capability to adapt different light sources to target analytes with different absorption spectra for colorimetric sensing.

ASSOCIATED CONTENT

Ⓢ Supporting Information

The Supporting Information is available free of charge on the ACS Publications website at DOI: 10.1021/acs.analchem.6b02484.

Comparison of cases with and without nanoLCA for protein quantification (PDF)

AUTHOR INFORMATION

Corresponding Authors
*E-mail: mgartia@lsu.edu.
*E-mail: loganliu@illinois.edu.
ORCID Ⓞ
Xinhao Wang: 0000-0002-4050-8736
Manas Ranjan Gartia: 0000-0001-6243-6780
Author Contributions
‖X.W. and T.W.C. contributed equally.
Notes
The authors declare no competing financial interest.

ACKNOWLEDGMENTS

REFERENCES

(1) Ament, I.; Prasad, J.; Henkel, A.; Schmachtel, S.; Sönnichsen, C. *Nano Lett.* **2012**, *12*, 1092−1095.

(2) Plucinski, L.; Gartia, M. R.; Arnold, W. R.; Ameen, A.; Chang, T.; Hsiao, A.; Liu, G. L.; Das, A. *Biosens. Bioelectron.* **2016**, *75*, 337−346.

(3) Rajasekharan, R.; Balaur, E.; Minovich, A.; Collins, S.; James, T. D.; Djalalian-Assl, A.; Ganesan, K.; Tomljenovic-Hanic, S.; Kandasamy, S.; Skafidas, E. *Scientific Reports*, vol. *4*, 2014.

(4) Yokogawa, S.; Burgos, S. P.; Atwater, H. A. *Nano Lett.* **2012**, *12*, 4349−4354.

(5) Gan, Q.; Bartoli, F. J.; Kafafi, Z. H. *Adv. Mater.* **2013**, *25*, 2385−2396.

(6) Shen, H.; Maes, B. *Opt. Express* **2011**, *19*, A1202−A1210.

(7) Chuang, S. L. *Physics of Photonic Devices*; John Wiley & Sons: 2012.

(8) Maier, S. A. *Plasmonics: Fundamentals and Applications*; Springer Science & Business Media: 2007.

(9) Dondapati, S. K.; Sau, T. K.; Hrelescu, C.; Klar, T. A.; Stefani, F. D.; Feldmann, J. *ACS Nano* **2010**, *4*, 6318−6322.

(10) Endo, T.; Yamamura, S.; Nagatani, N.; Morita, Y.; Takamura, Y.; Tamiya, E. *Sci. Technol. Adv. Mater.* **2005**, *6*, 491−500.

(11) Mayer, K. M.; Lee, S.; Liao, H.; Rostro, B. C.; Fuentes, A.; Scully, P. T.; Nehl, C. L.; Hafner, J. H. *ACS Nano* **2008**, *2*, 687−692.

(12) Vollmer, F.; Arnold, S. *Nat. Methods* **2008**, *5*, 591−596.

(13) Jung, L. S.; Campbell, C. T.; Chinowsky, T. M.; Mar, M. N.; Yee, S. S. *Langmuir* **1998**, *14*, 5636−5648.

(14) Brolo, A. G. *Nat. Photonics* **2012**, *6*, 709−713.

(15) Block, I. D.; Chan, L. L.; Cunningham, B. T. *Sens. Actuators, B* **2006**, *120*, 187−193.

(16) Shen, Y.; Zhou, J.; Liu, T.; Tao, Y.; Jiang, R.; Liu, M.; Xiao, G.; Zhu, J.; Zhou, Z.; Wang, X. *Nature Communications*, vol. *4*, 2013.

(17) Rakow, N. A.; Suslick, K. S. *Nature* **2000**, *406*, 710−713.

(18) Suslick, K. S.; Rakow, N. A.; Sen, A. *Tetrahedron* **2004**, *60*, 11133−11138.

(19) Janzen, M. C.; Ponder, J. B.; Bailey, D. P.; Ingison, C. K.; Suslick, K. S. *Anal. Chem.* **2006**, *78*, 3591−3600.

(20) Hong, J. I.; Chang, B. *Lab Chip* **2014**, *14*, 1725−1732.

(21) Shen, L.; Hagen, J. A.; Papautsky, I. *Lab Chip* **2012**, *12*, 4240−4243.

(22) Yetisen, A. K.; Martinez-Hurtado, J.; Garcia-Melendrez, A.; da Cruz Vasconcellos, F.; Lowe, C. R. *Sens. Actuators, B* **2014**, *196*, 156−160.

(23) Ebbesen, T. W.; Lezec, H. J.; Ghaemi, H.; Thio, T.; Wolff, P. *Nature* **1998**, *391*, 667−669.

(24) Gartia, M. R.; Hsiao, A.; Pokhriyal, A.; Seo, S.; Kulsharova, G.; Cunningham, B. T.; Bond, T. C.; Liu, G. L. *Adv. Opt. Mater.* **2013**, *1*, 1−1.

(25) Chang, T.; Wang, X.; Hsiao, A.; Xu, Z.; Lin, G.; Gartia, M. R.; Liu, X.; Liu, G. L. *Adv. Opt. Mater.* **2015**, *3*, 1397−1404.

(26) Seo, S.; Edwards, L.; Logan Liu, G. *Anal. Chem.* **2015**, *87*, 9710−9714.

(27) Brolo, A. G.; Gordon, R.; Leathem, B.; Kavanagh, K. L. *Langmuir* **2004**, *20*, 4813−4815.

(28) Chang, S.; Gray, S.; Schatz, G. *Opt. Express* **2005**, *13*, 3150−3165.

(29) Zhang, X.; Li, Z.; Ye, S.; Wu, S.; Zhang, J.; Cui, L.; Li, A.; Wang, T.; Li, S.; Yang, B. *J. Mater. Chem.* **2012**, *22*, 8903−8910.

(30) Yue, W.; Yang, Y.; Wang, Z.; Han, J.; Syed, A.; Chen, L.; Wong, K.; Wang, X. *J. Phys. D: Appl. Phys.* **2012**, *45*, 425401.

(31) Armbruster, D. A.; Pry, T. *Clin. Biochem. Rev.*, vol. *29*, Suppl 1, pp S49−52, Aug, **2008**.

(32) GISEN Group. *Lancet* **1997**, *349*, 1857−1863.